crystals

MDPI

Communication

SPS-Prepared High-Entropy $(Bi_{0.2}Na_{0.2}Sr_{0.2}Ba_{0.2}Ca_{0.2})TiO_3$ Lead-Free Relaxor-Ferroelectric Ceramics with High Energy Storage Density

Ya Lu [1,2], Haibo Zhang [2,3,4,5], Huabin Yang [6], Pengyuan Fan [2,3], Chanatip Samart [7], Naohisa Takesue [8] and Hua Tan [1,2,3,*]

1 State Key Laboratory of Digital Manufacturing Equipment and Technology, School of Mechanical Science and Engineering, Huazhong University of Science and Technology, Wuhan 430074, China
2 Guangdong Provincial Key Laboratory of Manufacturing Equipment Digitization, Guangdong HUST Industrial Technology Research Institute, Dongguan 523808, China
3 State Key Laboratory of Materials Processing and Die & Mould Technology, School of Materials Science and Engineering, Huazhong University of Science and Technology, Wuhan 430074, China
4 Faculty of Chemical Engineering, Industrial University of Ho Chi Minh City, Ho Chi Minh City 71420, Vietnam
5 Wenzhou Advanced Manufacturing Technology Research Institute of Huazhong University of Science and Technology, Wenzhou 325000, China
6 Guangxi Key Laboratory of Information Materials, Guilin University of Electronic Technology, Guilin 541004, China
7 Department of Chemistry, Faculty of Science and Technology, Thammasat University, Pathumthani 12120, Thailand
8 Faculty of Science, Fukuoka University, Fukuoka 814-0180, Japan
* Correspondence: hua_tan@hust.edu.cn

Abstract: Compared to batteries and electrochemical capacitors, dielectric capacitors are widely studied because of their huge advantages in terms of charging/discharging speed and power density. In this work, high-entropy $(Bi_{0.2}Na_{0.2}Sr_{0.2}Ba_{0.2}Ca_{0.2})TiO_3$ lead-free relaxor-ferroelectric ceramics were prepared by both conventional sintering (CS) and spark plasma sintering (SPS). The results showed that the ceramic prepared by SPS obtained a high energy storage density of 6.66 J/cm^3 and a satisfied energy storage efficiency of 77.2% under an electric field of 430 kV/cm. This is directly related to the high density, fine grains, number of oxygen vacancies, and composition uniformity of the SPS samples. This study provides a new path for the preparation of high-entropy dielectric energy storage ceramics with high energy storage properties.

Keywords: spark plasma sintering; dielectric ceramics; energy storage; relaxor-ferroelectrics

check for updates

Citation: Lu, Y.; Zhang, H.; Yang, H.; Fan, P.; Samart, C.; Takesue, N.; Tan, H. SPS-Prepared High-Entropy $(Bi_{0.2}Na_{0.2}Sr_{0.2}Ba_{0.2}Ca_{0.2})TiO_3$ Lead-Free Relaxor-Ferroelectric Ceramics with High Energy Storage Density. *Crystals* **2023**, *13*, 445. https://doi.org/10.3390/cryst13030445

Academic Editor: Alexei A. Bokov

Received: 14 February 2023
Revised: 23 February 2023
Accepted: 2 March 2023
Published: 4 March 2023

Copyright: © 2023 by the authors. Licensee MDPI, Basel, Switzerland. This article is an open access article distributed under the terms and conditions of the Creative Commons Attribution (CC BY) license (https://creativecommons.org/licenses/by/4.0/).

1. Introduction

Dielectric energy-storage capacitors have faster charge/discharge rates (- ns) and higher power densities (up to 108 W/kg) than batteries and electrochemical capacitors; they are important components of pulsed-power electronic systems, which are widely used in many applications, such as electric vehicles, medical defibrillators, photovoltaic power generation, ultra-high voltage DC transmission systems, electromagnetic catapults, electromagnetic guns, and spacecraft and satellites [1–3]. Among many dielectric materials, relaxor-ferroelectric (RFE) materials have high energy storage efficiency due to the presence of polar nano-regions (PNRs) instead of electric domains, so high recoverable energy storage density can be obtained, which has become a hot spot for research in recent years [4,5].

In 2015, Rost et al. [6] introduced the concept of high entropy to ceramic materials and successfully prepared (Mg,Ni,Cu,Co,Zn)O(RS) high-entropy ceramics with a uniform distribution of cations and obtained unique properties in terms of thermal conductivity. Since then, high-entropy ceramic materials have been reported to have excellent properties in terms

of high-temperature oxidation resistance [7,8], hardness [9,10], corrosion resistance [11,12], and dielectric properties [13–15]. In 2019, Pu et al. [14] synthesized a single-phase homogeneous A-site high-entropy $(Na_{0.2}Bi_{0.2}Ba_{0.2}Sr_{0.2}Ca_{0.2})TiO_3$ ceramic. It exhibited a relaxor behavior due to the disorder of the microscopic composition. Moreover, the recoverable energy storage density was 1.02 J/cm^3 under an electric field of 145 kv/cm. In 2020, Liu et al. [16] reported the dielectric energy storage properties of $(Bi_{0.2}Na_{0.2}K_{0.2}Ba_{0.2}Ca_{0.2})TiO_3$ high-entropy ceramics with relaxor-ferroelectric properties, but volatilization caused composition deviation and formation of a large number of oxygen vacancies. Moreover, due to the large difference in the sintering temperature of each component, the sample was not able to achieve complete densification, and the recoverable energy storage density and efficiency were only 0.684 J/cm^3 and 87.5%, respectively. In 2021, Liu et al. [17] prepared single-phase $(Bi_{1/6}Na_{1/6}Sr_{1/6}Ba_{1/6}Pb_{1/6}Ca_{1/6})TiO_3$ and $(Bi_{1/6}La_{1/6}Na_{1/6}K_{1/6}Sr_{1/6}Ba_{1/6})TiO_3$ high-entropy ceramics. The results confirmed the RFE behaviors. Xiong et al. [18] prepared a high-entropy RFE ceramic, $(Pb_{0.25}Ba_{0.25}Sr_{0.25}Ca_{0.25})TiO_3$, and found that the dielectric loss of the material was lower than 0.015 in temperature ranging from room temperature to 125 °C. In 2022, Yang and Zheng [19] prepared high-entropy ceramics $(Bi_{0.2}Na_{0.2}K_{0.2}La_{0.2}Sr_{0.2})TiO_3$ with a grain size as small as 45 nm, the recoverable energy storage density of which was 0.959 J/cm^3 under an electric field of 180 kV/cm. Due to the RFE behavior, in 2021, Zhou et al. [20] introduced a high-entropy compound, $Bi(Zn_{0.2}Mg_{0.2}Al_{0.2}Sn_{0.2}Zr_{0.2})O_3$, into $BaTiO_3$-$Na_{0.5}Bi_{0.5}TiO_3$ and obtained a high recoverable energy density of 3.74 J/cm^3 and a high energy storage efficiency of 82.2 %. Recently, an important breakthrough in energy storage ceramics based on the high entropy concept was achieved by Chen et al. [21]. By introducing (Li^+, Ba^{2+}, Bi^{3+}, Sc^{3+}, Hf^{4+}, Zr^{4+}, Ta^{5+}, Sb^{5+}) ions into the KNN lattice and using an advanced sintering technique, a local structure of R-O-T-C multiphase coexistence was obtained, thereby further refining the PNRs and obtaining a huge improvement in energy storage performance and efficiency with values of 10.06 J/cm^3 and 90.8%, respectively. Similarly, Yang et al. [22] designed a $(Bi_{3.25}La_{0.75})(Ti_{3-3x}Zr_xHf_xSn_x)O_{12}$ high-entropy system based on $Bi_4Ti_3O_{12}$ ceramic thin film to obtain a microstructure with the coexistence of nanograins and amorphous phases, and they obtained a huge energy storage density of 182 J/cm^3 under a 6360 kV/cm electric field, and 78% efficiency. These two works are of epoch-making significance for the research and application of high-entropy energy storage ceramics.

The biggest reason why high-entropy dielectric ceramics have low energy storage density is their low breakdown electric field (Eb). Due to their complex elemental composition, high-entropy dielectric ceramics are prone to elemental volatilization and component segregation during the preparation process, resulting in local performance degradation. At the same time, due to the huge difference in sintering activity between different components, it is difficult to realize the preparation of high-density, high-entropy dielectric ceramics by conventional sintering, which leads to a decrease in the breakdown electric field and energy storage density.

In this work, we designed $(Bi_{0.2}Na_{0.2}Sr_{0.2}Ba_{0.2}Ca_{0.2})TiO_3$ (BNSBCT) high-entropy dielectric ceramic according to the tolerance factor rule [23] and the principle of valence equilibrium. Two different sintering approaches, conventional sintering and spark plasma sintering, were used to compare the effect of microstructure on energy storage properties. The results showed that a high recoverable energy storage density of 6.66 J/cm^3 and an energy storage efficiency of 77.2% were obtained from the samples prepared by the SPS method, which provides a new path for fabricating high-performance dielectric energy-storage ceramics.

2. Materials and Methods

$(Bi_{0.2}Na_{0.2}Sr_{0.2}Ba_{0.2}Ca_{0.2})TiO_3$ powder was prepared by using the solid-state reaction. The experimental raw material powders were Bi_2O_3 (99%), $SrCO_3$ (99%), $CaCO_3$ (99%), $BaCO_3$ (99%), Na_2CO_3 (99.5%), and TiO_2 (98%) from Sinopharm Group Chemical Reagent Co., Ltd. First, the powders were mixed according to stoichiometry and then ball milled for 24 h with zirconia balls and ethanol (99%). After mixing, the powder was dried and

calcinated at 850 °C for 3 h. The calcinated powder was milled again for 24 h. For the conventional sintering, the calcinated powder was mixed with PVA as the binder and then pressed with a pressure of 10 MPa, and the green body was sintered at 1180 °C for 2 h with a heating rate of 5 °C/min in a muffle furnace. For spark plasma sintering (LABOX-1575, SINTER LAND Co., Nagaoka, Japan), the calcinated powder was placed in a graphite die with a diameter of 12 mm and heated to 900 °C with a heating rate of 100 °C/min under the pressure of 30 MPa; then, it was heated to 960 °C with a heating rate of 50 °C/min for 5 min. After cooling, the SPSed sample was heated in the air at 890 °C for 6 h to remove the graphite. The phase structures were determined by using X-ray diffraction (XRD) (XRD-7000 S, Kyoto, Japan, Shimadzu Co.). The grain morphology was observed with a scanning electron microscope (SEM) (FESEM, Eindhoven, Netherlands, Nova NanoSEM 450, FEI). The atomic arrangement in the lattice of the samples was observed by using a transmission electron microscopy (TEM, JEOL JEM2100, Tokyo, Japan) and a high-resolution transmission electron microscopy (HRTEM). The *P-E* hysteresis loops were measured on both unipolar and bipolar modes using a ferroelectric testing system (aixACCT Systems GmbH, Aachen, Germany).

3. Results and Discussion

From the X-ray diffraction pattern shown in Figure 1, it can be seen that the BNSBCT calcinated powder and the sintered samples all present a typical perovskite phase. At 31–32° and 38–40°, the calcinated powder displays an obvious double peak, which indicates a rhombohedral phase. For the XRD pattern of the sintered samples, there is only one peak at 30–31° and 38–40°, which indicates a cubic phase. Therefore, the symmetry of the perovskite structure is improved from a rhombohedral phase to a cubic phase after sintering. Moreover, the BNSBCT ceramics present a stable and single phase after sintering, and all the elements are located in the crystal lattice to form a high-entropy structure.

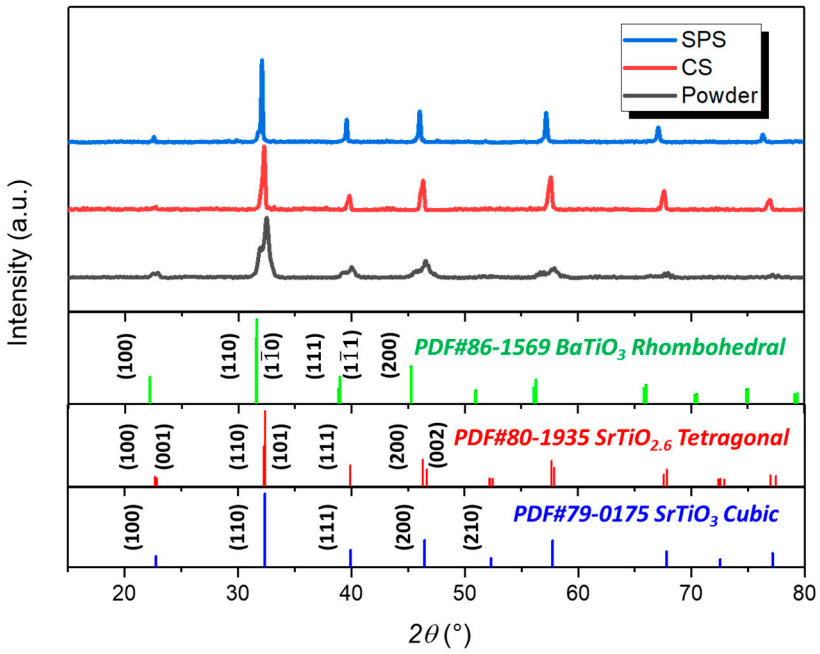

Figure 1. XRD patterns of the BNSBCT ceramic in different states: calcinated powder, conventionally sintered, and spark plasma sintered.

The microstructures of the BNSBCT ceramics prepared by conventional sintering and spark plasma sintering are shown in Figures 2a and 2b, respectively. The density and grain size distribution are also displayed on each figure. For the sample prepared by SPS, the density increases from 4.98 g/cm^3 to 5.04 g/cm^3, and the average grain size decreases from 0.77 μm to 0.52 μm. The higher densification of the sample prepared by SPS

derives from the mechanical pressure during the SPS process, which enhances the mass transportation between particles, while the finer grain size comes from two aspects. One is the lower sintering temperature: the sintering temperatures for conventional sintering and SPS are 1180 and 960 °C, respectively. Even if we consider the difference in the temperature measurement of the different sintering methods, the sintering temperature of SPS is still much lower than that of conventional sintering. The lower sintering temperature in SPS limits grain growth, leading to the formation of a microstructure with fine grains. The other one is the fast heating rate: the heating rates for conventional sintering and SPS are 5 °C/min and 100 °C/min (50 °C /min after 900 °C), respectively. The rapid heating during the initial sintering stage helps inhibit the coarsening of particles, thereby resulting in fine grains. Figure 2c presents the HR-TEM image of the BNSBCT ceramics prepared by SPS; it clearly shows that multiple different nano-regions are located in the same grain to form a short-term ordered and a long-term disordered state. Moreover, the dielectric properties of the BNSBCT ceramics prepared by CS and SPS are shown in Figure 2d. The dielectric permittivity for the CS and SPS samples increases and then decreases with increasing temperature, and the T_m (temperature at which the maximum dielectric constant is located) displays strong frequency dispersion, indicating a relaxor behavior. The dielectric permittivity of the SPS samples is obviously lower than that of the CS samples at all tested frequency. This is probably related to the grain size. The grain size of the SPS samples is finer than that of the CS samples, resulting in more grain boundaries in the SPS samples, which reduces the dielectric permittivity. In terms of the dielectric loss ($tg\delta$), at a low tested frequency, the dielectric permittivity of both sintering approaches shows little difference, with $tg\delta \sim 0.07$ at room temperature, which is slightly higher than the value reported in Pu's work [14]. At a high tested frequency, the $tg\delta$ of the SPS samples is 0.09 and 0.12 at the tested frequency of 100 kHz and 1 MHz, respectively, while the $tg\delta$ of the CS samples is 0.10 and 0.14 at the tested frequency of 100 kHz and 1 MHz, respectively. The fact that the $tg\delta$ of the SPS samples is lower than that of the CS samples indicates less defects and better energy storage properties in the SPS samples.

The unipolar *P-E* loops (the bipolar *P-E* loops can be seen in Figure S1) (see supplementary materials) of the two different sintering methods in Figure 3a show that the sample prepared by SPS has a significantly slimmer shape and a higher breakdown electric field. The breakdown electric field of the CS sample and the SPS sample is 250 kv/cm and 420 kv/cm, respectively. The conventional sintered sample obtains a recoverable energy storage density of 2.53 J/cm^3 and an energy storage efficiency of 56.8% under an electric field of 250 kV/cm. In contrast, the SPS-prepared sample achieves a recoverable energy storage density of 6.66 J/cm^3 and an energy storage efficiency of 77.2% under an electric field of 430 kV/cm. In Figure 3c, the energy storage density of the CS samples increases with increasing electric field, and the energy storage efficiency decreases from 90 to 56.8% with increasing electric field. For the SPS samples, the energy storage density follows the same trend as the CS samples. However, the energy storage efficiency stays around 80% until 300 kv/cm, and then increases to 80% again at 400 kv/cm. Figure 3e shows the *Pmax* and *Pr* of the BNSBCT samples prepared by CS and SPS, respectively. The *Pmax* of the SPS samples is obviously higher than that of the CS samples: the former reaches 57.2 μC/cm^2 under an electric field of 430 kv/cm and the latter reaches 34.9 μC/cm^2 under an electric field of 250 kv/cm, indicating a better energy storage property of the SPS samples. The *Pr* of the SPS samples is higher than that of the CS samples under an electric field of 190 kv/cm. When the electric field is higher than 190 kv/cm, the *Pr* of the CS samples increases rapidly and is higher than the SPS samples. This implies that the reversible nano domains of the SPS samples are more than those of the CS samples at a high electric field, resulting in a better energy storage property. Figure 3f shows the comparison of energy storage properties in previously reported high-entropy ceramics for energy storage applications [16,19–21,24–29]. The recoverable energy storage density of this work prepared by SPS is high among all

reported high-entropy ceramics, which indicates that the SPS method is a beneficial and important approach to fabricate high-entropy ceramics for energy storage applications.

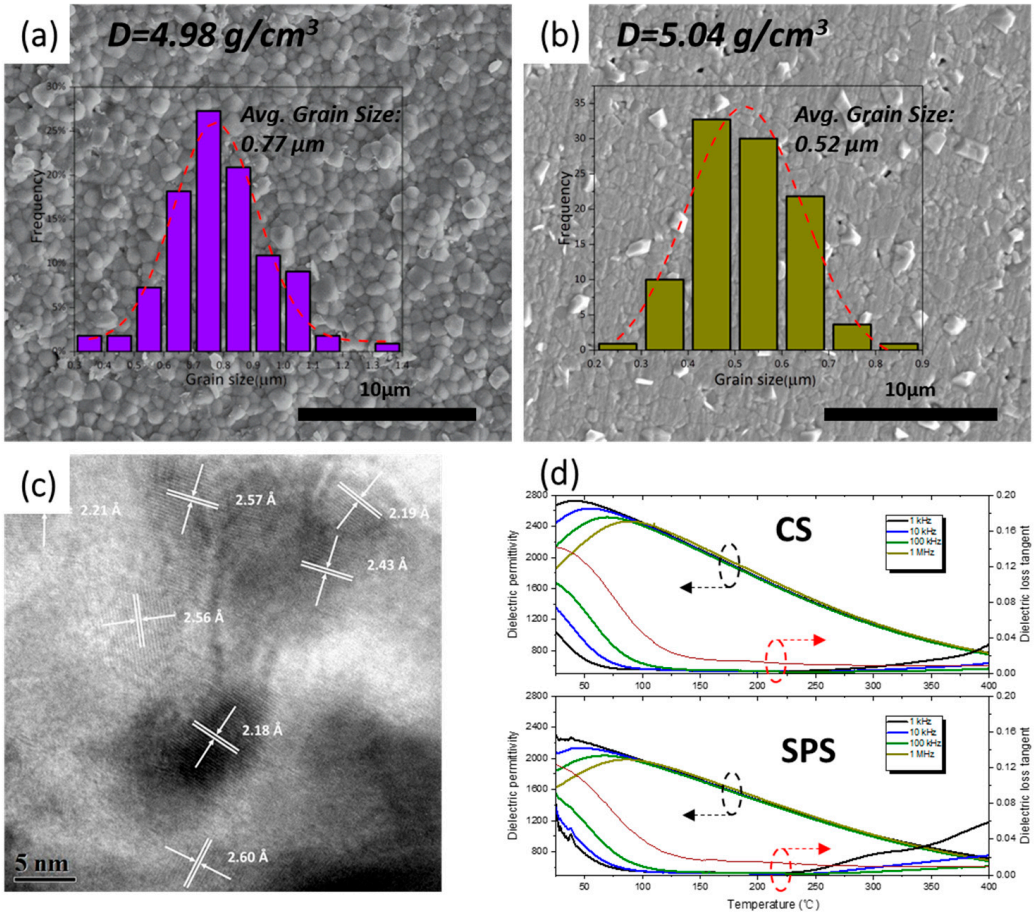

Figure 2. Microstructures of the BNSBCT ceramics prepared by different sintering methods: (**a**) conventional sintering, and (**b**) spark plasma sintering. (**c**) HR-TEM image and (**d**) dielectric properties of the BNSBCT ceramics prepared by CS and SPS.

The reasons for the high energy storage properties obtained for the SPS-prepared samples are as follows: First, the high densification of the SPS-prepared samples leads to a low sample porosity, which greatly avoids the electric field concentration on the pores of the samples, causing electric breakdown. This helps to enhance the high breakdown electric field. Second, due to the lower sintering temperature of SPS, the grains are finer than those sintered by conventional sintering. This leads to an increase in the number of grain boundaries. Since the dielectric constant of the grain boundaries is much lower than that of the grains, the local electric field in the grain boundaries is higher than that of the grains, and the breakdown will occur along the grain boundaries. The increase in the number of grain boundaries not only decreases the local electric field, but it also lengthens the breakdown path, thus increasing the breakdown electric field. Third, because the SPS method's sintering temperature and sintering time are much lower than those of conventional sintering, the volatilization of elements, such as Bi and Na, in the high-entropy composition is significantly reduced, resulting in a reduced number of oxygen vacancies in the samples and a uniform composition distribution, which results in a higher breakdown electric field as well as a higher energy storage efficiency.

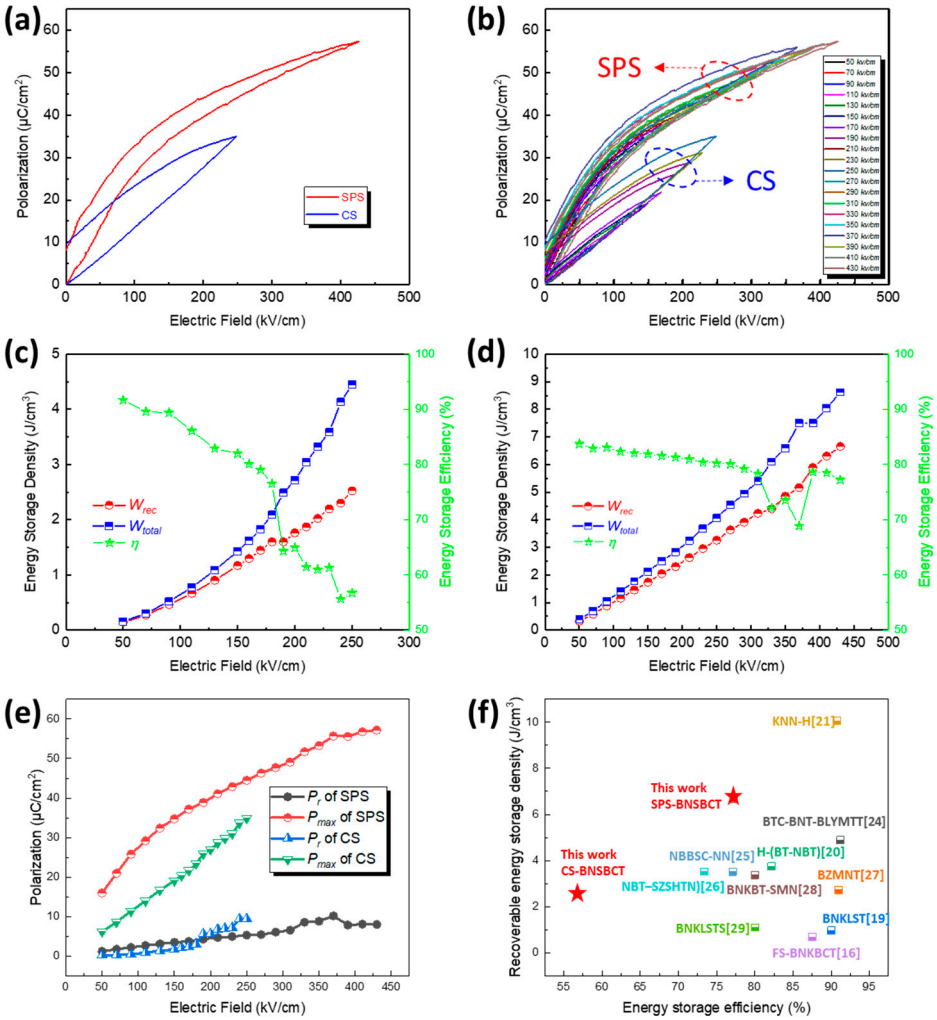

Figure 3. (**a**,**b**) *P-E* loops of the BNSBCT ceramics prepared by conventional sintering and SPS at varying electric field; (**c**,**d**) energy storage properties as a function of electric field for the BNSBCT ceramics prepared by CS and SPS; (**e**) Pr and Pmax as a function of electric field for the BNSBCT ceramics prepared by CS and SPS; and (**f**) a comparison of energy storage properties in previously reported high-entropy ceramics for energy storage applications [16,19–21,24–29].

4. Conclusions

In summary, due to the disadvantages of complex elements, difficult densification, and volatility of high-entropy perovskite materials, we successfully prepared high-density BNSBCT high-entropy ceramic materials with a fine grain size using the spark plasma sintering technique. The ceramics prepared by CS obtained a polarization of 34.9 μC/cm^2, an energy storage density of 2.53 J/cm^3, and an energy storage efficiency of 56.8% under an electric field of 250 kV/cm. In contrast, the ceramics prepared by SPS obtained a high polarization of 57.2 μC/cm^2, an energy storage density of 6.66 J/cm^3, and an energy storage efficiency of 77.2% under an electric field of 430 kV/cm. This is directly related to the high density, fine grains, number of oxygen vacancies, and composition uniformity of the SPS samples. This study provides a new path for the preparation of high-entropy dielectric energy storage ceramics with high energy storage properties.

Supplementary Materials: The following supporting information can be downloaded at: https://www.mdpi.com/article/10.3390/cryst13030445/s1, Figure S1: bipolar *P-E* loops of samples prepared by CS and SPS.

Author Contributions: Conceptualization, H.T., Y.L. and H.Z.; methodology, H.T., Y.L. and H.Y.; validation, P.F.; investigation, C.S.; data curation, Y.L.; writing—original draft preparation, Y.L.; writing—review and editing, H.T. and N.T.; supervision, H.T.; project administration, H.T. and H.Z.; funding acquisition, H.T. and H.Z. All authors have read and agreed to the published version of the manuscript.

Funding: This research was funded by the National Natural Science Foundation of China (No. 52202133), the Guangdong Basic and Applied Basic Research Foundation (2021A1515010025), the Dongguan Innovative Research Team Program (2020607101007), the Central Guidance for Local Science and Technology Development Funds (2021Szvup044), and the Basic Science and Technology Research Project of Wenzhou, Zhejiang Province (Grant Nos. G20210015). H.Z. also received financial support from the Bualuang ASEAN Chair Professor Research Grant.

Data Availability Statement: Not applicable.

Acknowledgments: The authors gratefully acknowledge the support provided by the National Natural Science Foundation of China (No. 52202133), the Guangdong Basic and Applied Basic Research Foundation (2021A1515010025), the Dongguan Innovative Research Team Program (2020607101007), the Central Guidance for Local Science and Technology Development Funds (2021Szvup044), and the Basic Science and Technology Research Project of Wenzhou, Zhejiang Province (Grant Nos. G20210015). H.Z. also acknowledged financial support from the Bualuang ASEAN Chair Professor Research Grant. The authors thank the Analytical and Testing Center of Huazhong University of Science and Technology for help in related tests.

Conflicts of Interest: The authors declare no conflict of interest.

References

1. Huang, S.; Liu, K.; Zhang, W.; Xie, B.; Dou, Z.; Yan, Z.; Tan, H.; Samart, C.; Kongparakul, S.; Takesue, N.; et al. All-Organic Polymer Dielectric Materials for Advanced Dielectric Capacitors: Theory, Property, Modified Design and Future Prospects. *Polym. Rev.* **2022**, *62*, 1–59. [CrossRef]
2. Zhang, H.; Wei, T.; Zhang, Q.; Ma, W.; Fan, P.; Salamon, D.; Zhang, S.T.; Nan, B.; Tan, H.; Ye, Z.G. A Review on the Development of Lead-Free Ferroelectric Energy-Storage Ceramics and Multilayer Capacitors. *J. Mater. Chem. C* **2020**, *8*, 16648–16667. [CrossRef]
3. Tan, H.; Yan, Z.; Chen, S.G.; Samart, C.; Takesue, N.; Salamon, D.; Liu, Y.; Zhang, H. SPS Prepared NN-24SBT Lead-Free Relaxor-Antiferroelectric Ceramics with Ultrahigh Energy-Storage Density and Efficiency. *Scr. Mater.* **2022**, *210*, 114428. [CrossRef]
4. Wei, T.; Liu, K.; Fan, P.; Lu, D.; Ye, B.; Zhou, C.; Yang, H.; Tan, H.; Salamon, D.; Nan, B.; et al. Novel $NaNbO_3$–$Sr_{0.7}Bi0\bullet 2TiO_3$ Lead-Free Dielectric Ceramics with Excellent Energy Storage Properties. *Ceram. Int.* **2021**, *47*, 3713–3719. [CrossRef]
5. Li, L.; Fan, P.; Wang, M.; Takesue, N.; Salamon, D.; Vtyurin, A.N.; Zhang, Y.; Tan, H.; Nan, B.; Lu, Y.; et al. Review of Lead-Free Bi-Based Dielectric Ceramics for Energy-Storage Applications. *J. Phys. D Appl. Phys.* **2021**, *54*, 293001. [CrossRef]
6. Rost, C.M.; Sachet, E.; Borman, T.; Moballegh, A.; Dickey, E.C.; Hou, D.; Jones, J.L.; Curtarolo, S.; Maria, J.P. Entropy-Stabilized Oxides. *Nat. Commun.* **2015**, *6*, 8485. [CrossRef] [PubMed]
7. Gild, J.; Zhang, Y.; Harrington, T.; Jiang, S.; Hu, T.; Quinn, M.C.; Mellor, W.M.; Zhou, N.; Vecchio, K.; Luo, J. High-Entropy Metal Diborides: A New Class of High-Entropy Materials and a New Type of Ultrahigh Temperature Ceramics. *Sci. Rep.* **2016**, *6*, 2–11. [CrossRef]
8. Wang, Z.; Li, Z.-T.; Zhao, S.-J.; Wu, Z.-G. High-Entropy Carbide Ceramics: A Perspective Review. *Tungsten* **2021**, *3*, 131–142. [CrossRef]
9. Moskovskikh, D.; Vorotilo, S.; Buinevich, V.; Sedegov, A.; Kuskov, K.; Khort, A.; Shuck, C.; Zhukovskyi, M.; Mukasyan, A. Extremely Hard and Tough High Entropy Nitride Ceramics. *Sci. Rep.* **2020**, *10*, 19874. [CrossRef] [PubMed]
10. Zhang, Y.; Sun, S.K.; Guo, W.M.; Zhang, W.; Xu, L.; Yuan, J.H.; Guan, D.K.; Wang, D.W.; You, Y.; Lin, H.T. Fabrication of Textured $(Hf_{0.2}Zr_{0.2}Ta_{0.2}Cr_{0.2}Ti_{0.2})B_2$ High-Entropy Ceramics. *J. Eur. Ceram. Soc.* **2021**, *41*, 1015–1019. [CrossRef]
11. Peng, Z.; Sun, W.; Xiong, X.; Zhang, H.; Guo, F.; Li, J. Novel Refractory High-Entropy Ceramics: Transition Metal Carbonitrides with Superior Ablation Resistance. *Corros. Sci.* **2021**, *184*, 109359. [CrossRef]
12. Dong, Y.; Ren, K.; Lu, Y.; Wang, Q.; Liu, J.; Wang, Y. High-Entropy Environmental Barrier Coating for the Ceramic Matrix Composites. *J. Eur. Ceram. Soc.* **2019**, *39*, 2574–2579. [CrossRef]
13. Zhou, S.; Pu, Y.; Zhang, Q.; Shi, R.; Guo, X.; Wang, W.; Ji, J.; Wei, T.; Ouyang, T. Microstructure and Dielectric Properties of High Entropy $Ba(Zr_{0.2}\ Ti_{0.2}Sn_{0.2}Hf_{0.2}Me_{0.2})O_3$ Perovskite Oxides. *Ceram. Int.* **2020**, *46*, 7430–7437. [CrossRef]
14. Pu, Y.; Zhang, Q.; Li, R.; Chen, M.; Du, X.; Zhou, S. Dielectric Properties and Electrocaloric Effect of High-Entropy $(Na_{0.2}Bi_{0.2}Ba_{0.2}Sr_{0.2}Ca_{0.2})TiO_3$ Ceramic. *Appl. Phys. Lett.* **2019**, *115*, 223901. [CrossRef]
15. Vinnik, D.A.; Trofimov, E.A.; Zhivulin, V.E.; Gudkova, S.A.; Zaitseva, O.V.; Zherebtsov, D.A.; Starikov, A.Y.; Sherstyuk, D.P.; Amirov, A.A.; Kalgin, A.V.; et al. High Entropy Oxide Phases with Perovskite Structure. *Nanomaterials* **2020**, *10*, 268. [CrossRef] [PubMed]

16. Liu, J.; Ren, K.; Ma, C.; Du, H.; Wang, Y. Dielectric and Energy Storage Properties of Flash-Sintered High-Entropy ($Bi_{0.2}Na_{0.2}K_{0\cdot2}Ba_{0.2}Ca_{0.2}$)$TiO_3$ Ceramic. *Ceram. Int.* **2020**, *46*, 20576–20581. [CrossRef]
17. Liu, W.; Li, F.; Chen, G.; Li, G.; Shi, H.; Li, L.; Guo, Y.; Zhai, J.; Wang, C. Comparative Study of Phase Structure, Dielectric Properties and Electrocaloric Effect in Novel High-Entropy Ceramics. *J. Mater. Sci.* **2021**, *56*, 18417–18429. [CrossRef]
18. Xiong, W.; Zhang, H.; Cao, S.; Gao, F.; Svec, P.; Dusza, J.; Reece, M.J.; Yan, H. Low-Loss High Entropy Relaxor-like Ferroelectrics with A-Site Disorder. *J. Eur. Ceram. Soc.* **2021**, *41*, 2979–2985. [CrossRef]
19. Yang, W.; Zheng, G. High Energy Storage Density and Efficiency in Nanostructured ($Bi_{0.2}Na_{0.2}$ $K_{0.2}La_{0.2}Sr_{0.2}$)TiO_3 High-Entropy Ceramics. *J. Am. Ceram. Soc.* **2022**, *105*, 1083–1094. [CrossRef]
20. Zhou, S.; Pu, Y.; Zhang, X.; Shi, Y.; Gao, Z.; Feng, Y.; Shen, G.; Wang, X.; Wang, D. High Energy Density, Temperature Stable Lead-Free Ceramics by Introducing High Entropy Perovskite Oxide. *Chem. Eng. J.* **2022**, *427*, 131684. [CrossRef]
21. Chen, L.; Deng, S.; Liu, H.; Wu, J.; Qi, H.; Chen, J. Giant Energy-Storage Density with Ultrahigh Efficiency in Lead-Free Relaxors via High-Entropy Design. *Nat. Commun.* **2022**, *13*, 3089. [CrossRef] [PubMed]
22. Yang, B.; Zhang, Y.; Pan, H.; Si, W.; Zhang, Q.; Shen, Z.; Yu, Y.; Lan, S.; Meng, F.; Liu, Y.; et al. High-Entropy Enhanced Capacitive Energy Storage. *Nat. Mater.* **2022**, *21*, 1074–1080. [CrossRef]
23. Goldschmidt, V.M. Die Gesetze Der Krystallochemie. *Naturwissenschaften* **1926**, *14*, 477–485. [CrossRef]
24. Li, Z.; Chen, Z.; Xu, J. Enhanced Energy Storage Performance of $BaTi_{0.97}Ca_{0.03}O_{2.97}$-Based Ceramics by Doping High-Entropy Perovskite Oxide. *J. Alloys Compd.* **2022**, *922*, 166179. [CrossRef]
25. Ning, Y.; Pu, Y.; Wu, C.; Zhou, S.; Zhang, L.; Zhang, J.; Zhang, X.; Shang, Y. Enhanced Capacitive Energy Storage and Dielectric Temperature Stability of A-Site Disordered High-Entropy Perovskite Oxides. *J. Mater. Sci. Technol.* **2023**, *145*, 66–73. [CrossRef]
26. Zhou, S.; Pu, Y.; Zhao, X.; Ouyang, T.; Ji, J.; Zhang, Q.; Zhang, C.; Sun, S.; Sun, R.; Li, J.; et al. Dielectric Temperature Stability and Energy Storage Performance of NBT-based Ceramics by Introducing High-entropy Oxide. *J. Am. Ceram. Soc.* **2022**, *105*, 4796–4804. [CrossRef]
27. Chen, Y.; Qi, J.; Zhang, M.; Luo, Z.; Lin, Y.H. Pyrochlore-Based High-Entropy Ceramics for Capacitive Energy Storage. *J. Adv. Ceram.* **2022**, *11*, 1179–1185. [CrossRef]
28. Yan, B.; Chen, K.; An, L. Design and Preparation of Lead-Free ($Bi_{0.4}Na_{0.2}K_{0.2}Ba_{0.2}$)$TiO_3$-Sr($Mg_{1/3}Nb_{2/3}$)$O_3$ High-Entropy Relaxor Ceramics for Dielectric Energy Storage. *Chem. Eng. J.* **2023**, *453*, 139921. [CrossRef]
29. Yang, W.; Zheng, G. Tunning the Dielectric and Energy Storage Properties of High Entropy Ceramics (Bi0.2Na0.2K0.2La0.2Sr0.2)(Ti1-XScx)O3 by Sc-Doping at B-Site in Perovskite Structure. *J. Electroceramics* **2022**, *49*, 53–62. [CrossRef]

Disclaimer/Publisher's Note: The statements, opinions and data contained in all publications are solely those of the individual author(s) and contributor(s) and not of MDPI and/or the editor(s). MDPI and/or the editor(s) disclaim responsibility for any injury to people or property resulting from any ideas, methods, instructions or products referred to in the content.